SCIENCE CHINA
Physics, Mechanics & Astronomy

• Article •

April 2024 Vol. 67 No. 4: 240511
https://doi.org/10.1007/s11433-023-2303-7

Uncovering hidden nodes and hidden links in complex dynamic networks

Zhaoyang Zhang[1†], Xinyu Wang[2,3†], Haihong Li[2], Yang Chen[4], Zhilin Qu[3*], Yuanyuan Mi[5*], and Gang Hu[6*]

[1] *Department of Physics, School of Physical Science and Technology, Ningbo University, Ningbo 315211, China;*
[2] *School of Science, Beijing University of Posts and Telecommunications, Beijing 100876, China;*
[3] *Department of Medicine, David Geffen School of Medicine, University of California, Los Angeles 90095, USA;*
[4] *Brainnetome Center and National Laboratory of Pattern Recognition, Institute of Automation, Chinese Academy of Sciences, Beijing 100190, China;*
[5] *Department of Psychology, Tsinghua University, Beijing 100084, China;*
[6] *Department of Physics, Beijing Normal University, Beijing 100875, China*

Received September 5, 2023; accepted December 20, 2023; published online March 1, 2024

Inferring network structures from available data has attracted much interest in network science; however, in many realistic networks, only some of the nodes are perceptible while others are hidden, making it a challenging task. In this work, we develop a method for reconstructing the network with hidden nodes and links, taking account of fast-varying noise and time-delay interactions. By calculating the correlations of available data with different derivative orders for multiple pairs of accessible nodes, analyzing and integrating the relationships between different correlations, and defining diverse hidden-node-related reconstruction motifs, we can effectively identify the hidden nodes and hidden links in the network.

networks and genealogical trees, stochastic analysis methods, time series analysis

PACS number(s): 89.75.Hc, 05.10.Gg, 05.45.Tp

Citation: Z. Zhang, X. Wang, H. Li, Y. Chen, Z. Qu, Y. Mi, and G. Hu, Uncovering hidden nodes and hidden links in complex dynamic networks, Sci. China-Phys. Mech. Astron. **67**, 240511 (2024), https://doi.org/10.1007/s11433-023-2303-7

1 Introduction

The structure of a complex network is closely associated with its functions, and thus, revealing the network structure is crucial to understanding and controlling its behaviors. In practice, one can observe the activities of a network by measuring output data of certain network units (e.g., nodes), but the network structure is often not directly detectable. Hence, inferring the network structure from measurable data, i.e., network reconstruction, becomes a critical task [1-14]. In neuroscience, inference of some practical neural networks with experimental data has been performed [15-18]. The major difficulty in network reconstruction is data shortage, namely, some nodes or links are not accessible or are hidden, data of which are not measurable. Thus, inferring network structures by analysis of accessible data only and uncovering hidden nodes becomes a challenging task. Many approaches to extracting information about hidden nodes have been performed in different kinds of networks, such as ascertaining existence of a hidden node together with its accessible neighbors [19-21]; detecting the total number of hidden nodes in a given network [22,23]; describing the effects of hidden nodes for network inferences [24-26]; inferring hidden nodes and their interaction structure for spin systems with known tran-

*Corresponding authors (Zhilin Qu, email: zqu@mednet.ucla.edu; Yuanyuan Mi, email: miyuanyuan0102@163.com; Gang Hu, email: ganghu@bnu.edu.cn)

† These authors contributed equally to this work.

sition probability [27-29]; and reconstructing interactions between two accessible nodes linked through distant paths with all nodes in between hidden nodes, by analysis of the data of these two nodes only [30, 31]. Despite all the above efforts, reconstruction of the dark world associated with multiple hidden nodes with totally unknown interactions and network dynamics still lacks clarity.

In this paper, by calculating different orders of correlations between available data of accessible nodes, integrating the correlation results obtained from multiple pairs of different accessible nodes, and defining diverse hidden-node-related reconstruction motifs, hidden nodes can be recognized and discriminated, links among accessible and hidden nodes in the network can be inferred, and rich information regarding intensities and time delays of all detected links can be extracted. In this work, two key points, namely, the presence of fast-varying noises and time-delay for signal propagation through interactions in the network, are considered. Generally, these two factors are pervasive in realistic systems [32-36] and they can bring difficulties in analyzing network behaviors by generating random fluctuations and making network dynamics more complicated [37-40]. In this work, we present that these factors are greatly helpful in examining hidden nodes and the associated dark network structure.

2 Uncovering hidden nodes and hidden structure by applying noise injection: theory and method

Neural networks have attracted huge attention in practice, where a number of units are often not accessible while important for realistic functions of neural systems [41-46]. Let us consider a neural network with the units described by the Bär model [47, 48]

$$\frac{\mathrm{d}x_i(t)}{\mathrm{d}t} = -\frac{1}{\varepsilon}x_i(t)(x_i(t)-1)\Big(x_i(t)-\frac{y_i(t)+b}{a}\Big) + \sum_{j=1,j\neq i}^{N} w_{ij}\Big(x_j\left(t-\hat{\tau}_{ij}\right)-x_i\left(t\right)\Big),\ i=1,2,\cdots,N, \tag{1a}$$

$$\frac{\mathrm{d}y_i(t)}{\mathrm{d}t} = f\left(x_i\left(t\right)\right)-y_i(t), \tag{1b}$$

$$f(x_i) = \begin{cases} 0, & x_i < \frac{1}{3}, \\ 1-6.75x_i\left(x_i-1\right)^2, & -\frac{1}{3} \le x_i \le 1, \\ 1, & x_i > 1, \end{cases} \tag{1c}$$

where x_i and y_i refer to the membrane potential and recovery variable of neuron i, respectively, and w_{ij} $(j\neq i)$ represents the coupling intensity from node j to node i with $\hat{\tau}_{ij}$ being interaction time-delay, if this direct interaction exists. Figure 1(a) illustrates an example of an artificial network with $N = 8$, where $M = 6$ red nodes are accessible, that is, their data can be measured, and certain signals can be injected, and $N - M = 2$ black nodes and all black links are hidden. The task is to detect the hidden nodes and infer all links with available data of accessible nodes only. To do so, white noise is injected into an accessible node, for example, node A, and the data of two accessible nodes A and B $(B\neq A)$ are measured, then the differential equation for A is changed to

$$\frac{\mathrm{d}x_A(t)}{\mathrm{d}t} = -\frac{1}{\varepsilon}x_A(t)(x_A(t)-1)\Big(x_A(t)-\frac{y_A(t)+b}{a}\Big) + \sum_{j=1,j\neq A}^{N} w_{Aj}\Big(x_j(t-\hat{\tau}_{Aj})-x_A\left(t\right)\Big)+\Gamma_A(t), \tag{2a}$$

where noise $\Gamma_A(t)$ injected to node A is the signal that provides rich information on the hidden structure in the network, as shown below. The noise has a correlation time much smaller than the characteristic time of network dynamics, and is approximated by white noise, satisfying

$$\langle\Gamma_A(t)\rangle = 0; \langle\Gamma_A(t)\Gamma_A(t+t')\rangle = Q_A\delta(t'). \tag{2b}$$

The outputs from A and B are

$$\begin{aligned} &x_A(t_1), x_A(t_2), \cdots, x_A(t_k), \cdots, x_A(t_L), \\ &x_B(t_1), x_B(t_2), \cdots, x_B(t_k), \cdots, x_B(t_L), \end{aligned} \tag{2c}$$

with the sampling interval $\triangle t$

$$0 < \triangle t = t_{k+1} - t_k \ll 1 \text{ for } k = 1, 2, \cdots, L-1.$$

A and B can be selected among all the accessible nodes of Figure 1(a).

Rich information about the network structure can be extracted by diverse correlation calculations with data of $x_A(t)$ and $x_B(t)$ as:

$$C_{BA}^{\nu,1}(t' = k'\Delta t) = \frac{1}{L}\sum_{k=1}^{L} x_B^{(\nu)}(t_{k+k'})x_A^{(1)}(t_k), \tag{3}$$

where $x_i^{(\nu)}$ is the νth-order "derivative" of x_i, defined by

$$x_i^{(\nu)}(t_k) = \frac{x_i^{(\nu-1)}(t_{k+1}) - x_i^{(\nu-1)}(t_k)}{\Delta t}, x_i^{(0)}(t_k) = x_i(t_k).$$

We take $x_i(t_k) = 0$ for all $k \le 0$ and $k > L$. In eq. (3) correlations for different $\nu's$ include various and often mutually independent information. If there is an interaction path from A to B with distance d, we have

$$\hat{I}_{BA}(d) = w_{j_1A}\prod_{\mu=2}^{d-1} w_{j_\mu j_{\mu-1}} w_{Bj_{d-1}}, \tag{4a}$$

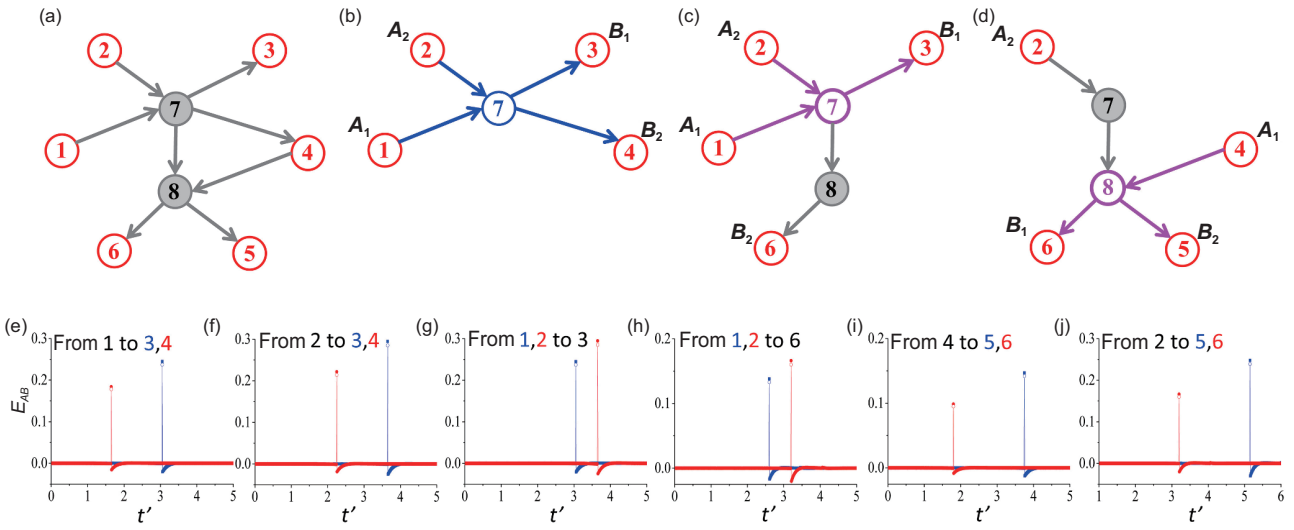

Figure 1 Reconstruction of a simple network described by eqs. (1) and (2) through reconstruction motifs. $a = 0.84$, $b = 0.07$, $\varepsilon = 0.04$, and $Q_A = 0.2$. All direct interactions w_{ij} take values in (0.8, 1.2) and time-delay $\hat{\tau}_{ij}$ in (0.2, 1) with equal probabilities. (a) Network structure under consideration. Nodes 7, 8 and all links are hidden (black nodes and links). (b)-(d) Three network motifs used for inferring hidden nodes and hidden links by using eq. (6). Namely, we can definitely identify the hidden nodes (node 7 in (b), 7 in (c) and 8 in (d)), the colored links (blue colored in (b) and purple colored in (c) and (d), and differentiate them from the remaining hidden nodes and hidden links). (e)-(j) Some correlations between given pairs of accessible nodes A and B ($B \neq A$), $E_{BA}^{d+1,1}(t')$'s plotted against t' ((e), (f) for motif (b); (g), (h) for motif (c); and (i), (j) for motif (d)). All circles indicate actual interaction intensities $Q_A\hat{I}_{BA}(d)$ (vertical heights) and actual total time delays $\hat{\tau}_{BA}(d)$ (horizontal t'*s* positions of circles) along the interaction paths, which overlap accurately with the reconstructed ones (peak height $Q_A I_{BA}(d)$ and peak positions $\tau_{BA}(d)$). The network structure in (a) is fully reconstructed by applying network motifs in (b)-(d). Note that node 7 and blue links are inferred by the motif in (b), and the hidden node 7 (8) and all purple links are inferred by the motif in (c) ((d)) through identities in eqs. (6a) and (6b) (eqs. (6c) and (6d)).

$$\hat{\tau}_{BA}(d) = \hat{\tau}_{j_1 A} + \sum_{\mu=2}^{d-1} \hat{\tau}_{j_\mu j_{\mu-1}} + \hat{\tau}_{B j_{d-1}}, \tag{4b}$$

where $\hat{I}_{BA}(d)$, $\hat{\tau}_{BA}(d)$ indicates the actual interaction intensity and total time delay along the path of length d

$$A \to j_1 \to \cdots \to j_\mu \to \cdots \to j_{d-1} \to B. \tag{4c}$$

Based on eqs. (1) and (4) and for an actual interaction path from node A to node B with distance d, we have

$$x_B^{(d+1)}(t) = \hat{I}_{BA}(d) x_A^{(1)}(t - \hat{\tau}_{BA}(d)) + \text{other terms}.$$

Eq. (3) can be further derived to

$$\begin{aligned} E_{BA}^{\nu=d+1,1}(t') =& C_{BA}^{d+1,1}(t')\Delta t \\ =& \begin{cases} 0(\Delta t), & t'_k \neq \hat{\tau}_{BA}(d); \\ Q_A \hat{I}_{BA}(d) + 0(\Delta t), & t'_k = \hat{\tau}_{BA}(d). \end{cases} \end{aligned} \tag{5}$$

Hence, the interaction from A to B of $\hat{I}_{BA}(d)$ and $\hat{\tau}_{BA}(d)$ can be inferred from accessible data of nodes A and B by computation of the peak height $\hat{I}_{BA}(d) \approx I_{BA}(d)$ and peak position $\hat{\tau}_{BA}(d) \approx \tau_{BA}(d)$ in eq. (5), where $I_{BA}(d)$ and $\tau_{BA}(d)$ refer to the reconstructed interaction intensity and total time delay along the path, respectively [30, 49, 50].

By analysis of the output data of the accessible nodes of eq. (2c), rich information on paths can be extracted with different distances using eqs. (4) and (5) from $d = 1$ to, in principle, any large d if data of sufficiently large length $L \gg 1$ and small enough sampling interval $\Delta t \ll 1$ are available. In addition, this information can be employed to infer interaction structure in networks not only between accessible nodes ($d = 1$), but also between accessible and hidden nodes ($d = 2$), and even between hidden nodes ($d \geq 3$).

We demonstrate the results of the above analyses by computing a simple network structure in Figure 1(a) with data of accessible nodes only. Figure 1(e)-(j) present some cases of $E_{BA}^{d+1,1}(t')$ calculated from eq. (5) for several $d = 2$ and $d = 3$ pairs with nonzero peaks. In Figure 1(b), (e), (f), it can be concluded that there is definitely one hidden node along each interaction path $1 \to 3, 4$ and $2 \to 3, 4$. Without further analysis, the four peaks in Figure 1(e) and (f) may be associated with any of the four cases from one to four hidden nodes. However, by integrating the correlations of all the four peaks in addition to appropriate computation and derivation, we conclude definitely that all the four paths pass through a single hidden node (say node 7). For instance, by comparing the peak heights (identifying $Q_A I_{BA}(d)$) and peak positions (showing $\tau_{BA}(d)$), we can convincingly reach the above conclusion, that is, if equalities

$$\begin{aligned} &\tau_{B_1A_1}(d=2) - \tau_{B_1A_2}(d=2) = \tau_{B_2A_1}(d') - \tau_{B_2A_2}(d') \\ &= \tau_{h_1A_1}(1) - \tau_{h_1A_2}(1) \approx \hat{\tau}_{h_1A_1}(1) - \hat{\tau}_{h_1A_2}(1), \end{aligned} \tag{6a}$$

$$\begin{aligned} &I_{B_1A_1}(d=2)/I_{B_1A_2}(d=2) = I_{B_2A_1}(d')/I_{B_2A_2}(d') \\ &= I_{h_1A_1}(1)/I_{h_1A_2}(1) \approx \hat{I}_{h_1A_1}(1)/\hat{I}_{h_1A_2}(1) \end{aligned} \tag{6b}$$

are justified, a hidden node h_1 and its inputs from A_1 and A_2 nodes can be determined; and if equations

$$\tau_{B_1A_1}(d=2)-\tau_{B_2A_1}(d=2)=\tau_{B_1A_2}(d')-\tau_{B_2A_2}(d') \\ =\tau_{B_1h_2}(1)-\tau_{B_2h_2}(1)\approx\hat{\tau}_{B_1h_2}(1)-\hat{\tau}_{B_2h_2}(1), \tag{6c}$$

$$I_{B_1A_1}(d=2)/I_{B_2A_1}(d=2)=I_{B_1A_2}(d')/I_{B_2A_2}(d') \\ =I_{B_1h_2}(1)/I_{B_2h_2}(1)\approx\hat{I}_{B_1h_2}(1)/\hat{I}_{B_2h_2}(1) \tag{6d}$$

are valid, a single hidden node h_2 and its outputs to nodes B_1 and B_2 can be inferred. In eq. (6), all these $d-1$ and $d'-1$ nodes are hidden in the considered paths. It can be easily verified that the four peaks of Figure 1(e) and (f) satisfy all eqs. (6a)-(6d) with $d=d'=2$, $A_1=1$, $A_2=2$, $B_1=3$, $B_2=4$, and identify $h_1=h_2=7$ and its inputs and outputs by blue color shown in Figure 1(b). The four peaks of Figure 1(g) and (h) satisfy eqs. (6a) and (6b) with $d=2$, $d'=3$, $A_1=1$, $A_2=2$, $B_1=3$, $B_2=6$, and determine $h_1=7$ and its inputs and outputs by purple color as shown in Figure 1(c). The four peaks of Figure 1(i) and (j) justify eqs. (6c) and (6d) with $d=2$, $d'=3$, $A_1=4$, $A_2=2$, $B_1=6$, $B_2=5$, and identify $h_2=8$ and its input and outputs by purple color as shown in Figure 1(d). With substructure, the motif in Figure 1(b), hidden node 7 can uniquely be identified, that is, identify node 7 and all its inputs from observable nodes and outputs to observable nodes from all the rest of the hidden nodes and other links. The motif in Figure 1(c) (Figure 1(d)) determines hidden node 7 (8) and identifies the hidden node and its inputs (outputs) links with observable nodes from any other hidden nodes and hidden links. Hence, the simplest detectable structure is distinguished as a reconstruction motif, with which a hidden node and some of its links with accessible nodes can be recognized according to the analysis of measured accessible node data in the motif. In this work, three different motifs are shown in Figure 1(b)-(d), with which we can evidently distinguish all hidden nodes and hidden links in the network of Figure 1(a). Some more complex motifs with distant interaction paths are displayed in Appendix Figure a1.

3 Uncovering hidden nodes and hidden structure by applying noise injection: numerical demonstration

We demonstrate the above in a simple network how to use noise injection and analyze output data of the accessible nodes to uncover hidden nodes and links. This method can be directly extended to more complex and larger networks by utilizing the network motifs in Figure 1(b)-(d). A complex network of size $N=20$ is illustrated in Figure 2(a). In this network, ten red nodes (Figure 2(b)) are accessible, while all the other black nodes in Figure 2(a) are hidden, and the interaction structures of the whole network and network dynamics are all unknown. The time series (e.g., eq. (2c)) of the accessible nodes are generated using eqs. (1) and (2) with noise being injected to one of the accessible nodes (i.e., node A in Figure 2(b)). The aim is network reconstruction, that is, to explore additional hidden nodes in Figure 2(a) and infer hidden links associated with these uncovered nodes.

Based on the correlation results of $d=1$ [50], all direct interactions between accessible nodes (red arrows in Figure 2(c)) can be easily investigated. The reconstructed results of $I_{BA}(d)$ and $\tau_{BA}(d)$ for all pairs of $d=2$ ($A,B=1,2,...,10$) are listed in Table a1 and those for $d=3$ are in Table a2 by quantities of Roman type. In addition, hidden nodes and links can be inferred by using $E_{BA}^{d+1,1}(t')$ with $d=2$ (blue nodes and links in Figure 2(d) and blue numbers in Table a3) through motif in Figure 1(b) and by using $E_{BA}^{d+1,1}(t')$ with $d=2,3$ (purple nodes and links in Figure 2(e) and purple numbers in Tables a3 and a4) based on motifs in Figure 1(c) and (d). For example, by integrating the results in Tables a1 and a2 and systematically applying eqs. (6) with network motifs in Figure 1(b)-(d), we obtain the structures of Figure 2(d) and (e) step by step, fully reconstructing network of Figure 2(a). In Figure 2(f) and (g), we plot ratio of intensities $R=\frac{I_{h_\mu A_1}}{I_{h_\mu A_2}}$ and time delay differences $\Delta\tau=\tau_{h_\mu A_1}-\tau_{h_\mu A_2}$ between any pairs of inputs and also $R=\frac{I_{B_1h_\mu}}{I_{B_2h_\mu}}$ and $\Delta\tau=\tau_{B_1h_\mu}-\tau_{B_2h_\mu}$ for outputs with $\mu=1,2,\cdots,N-M$ for all hidden nodes, and compare these reconstructed values with actual ones ($\hat{R}=\frac{\hat{I}_{h_\mu A_1}}{\hat{I}_{h_\mu A_2}}$ or $\hat{R}=\frac{\hat{I}_{B_1h_\mu}}{\hat{I}_{B_2h_\mu}}$ and $\Delta\hat{\tau}=\hat{\tau}_{h_\mu A_1}-\hat{\tau}_{h_\mu A_2}$ or $\Delta\hat{\tau}=\hat{\tau}_{B_1h_\mu}-\hat{\tau}_{B_2h_\mu}$). All dots distribute along the diagonal lines, confirming acceptable reconstruction of these network quantities. It should be indicated that for each hidden node, two arbitrary factors, one for time delays and the other for interaction intensity, are not determined. Note that network in Figure 2(e) has 50% hidden nodes and more than 85% links output from or input to hidden nodes. It is a fascinating success for us to conclude the complete reconstruction.

In Figure 2(e) and Tables a3, a4, all the hidden nodes and hidden links of network in Figure 2(a) have been reconstructed by employing the motifs in Figure 1(b)-(d) only. With a given network, a larger ratio of hidden nodes relative to observable nodes can certainly render the task of uncovering the hidden structure more difficult. In these cases, the calculation of additional correlations of data of measurable nodes and identification of additional motifs with larger $d's$ (e.g., $d>3$) (such as those in Figure a1 and others) may help us in full reconstruction. Nevertheless, the conditions for complete reconstruction (such as the requirements of the ratio of accessible nodes relative to hidden nodes, link density, and network structures) are still significant, which warrants further investigation.

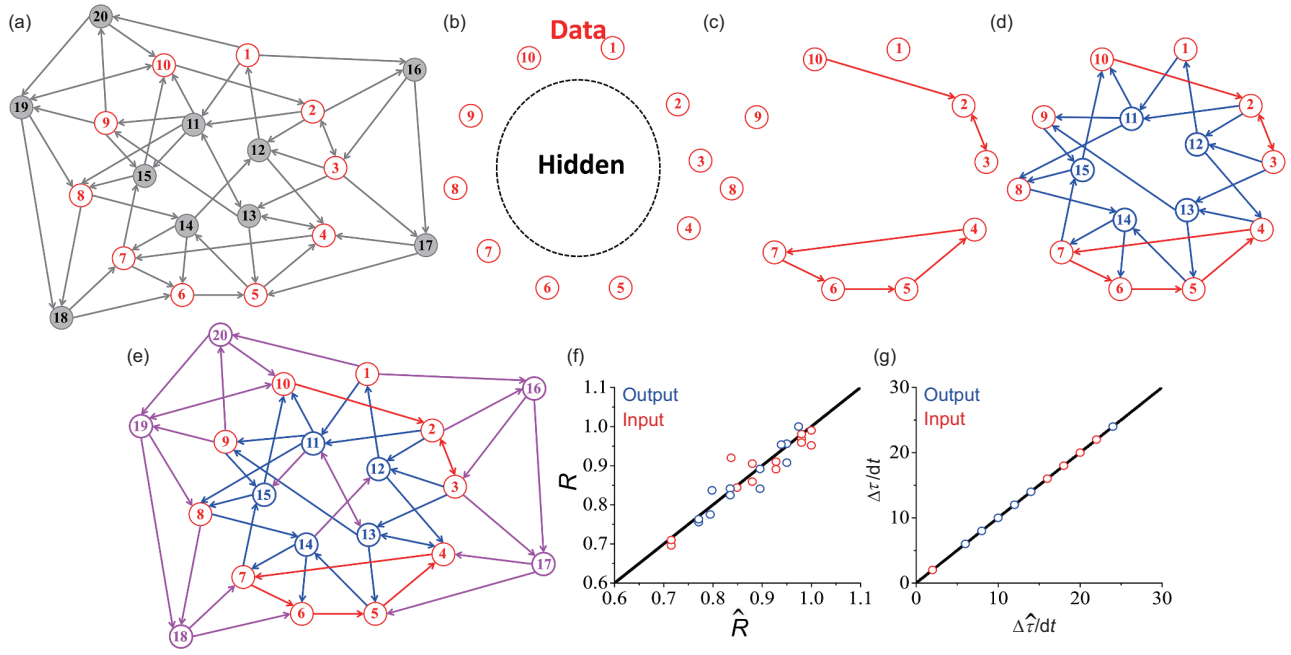

Figure 2 Reconstruction of a complex network with excitable dynamics described by eqs. (1) and (2). Each node has probability $P = 0.25$ to have input from or output to another node, and all other parameters are the same as in Figure 1. (a) Network to be reconstructed. All black nodes and links are unknown, and the network dynamics are unknown either. (b) Accessible nodes with measurable data and noise injection applicable. (c) By analysis of $d = 1$ correlations of eqs. (3)-(5), direct interactions between accessible nodes can be inferred by red arrows. (d) By integration of $d = 2$ correlations in Table a1 and application of the network motif in Figure 1(b), some hidden nodes and the associated links are inferred by blue nodes and blue arrows (blue numbers in Table a3). (e) By integration of the results of both $d = 2$ and $d = 3$ in Tables a1, a2 and application of the network motifs in Figure 1(c) and (d), all the rest of the hidden nodes and their interaction structure are inferred by purple nodes and purple arrows (purple quantities in Tables a3, a4). (f) Ratios of reconstructed intensities between any pairs of inputs ($R = \frac{I_{h_\mu A_1}}{I_{h_\mu A_2}}$ for red circles) and outputs ($R = \frac{I_{B_1 h_\mu}}{I_{B_2 h_\mu}}$ for blue circles) for each given hidden nodes are plotted against actual ones ($\hat{R} = \frac{\hat{I}_{h_\mu A_1}}{\hat{I}_{h_\mu A_2}}$ or $\hat{R} = \frac{\hat{I}_{B_1 h_\mu}}{\hat{I}_{B_2 h_\mu}}$). (g) Same as (f) with differences of reconstructed time delays plotted ($\Delta\tau = \tau_{h_\mu A_1} - \tau_{h_\mu A_2}$ for red dot and $\Delta\tau = \tau_{B_1 h_\mu} - \tau_{B_2 h_\mu}$ for blue dots versus actual ones $\Delta\hat{\tau} = \hat{\tau}_{h_\mu A_1} - \hat{\tau}_{h_\mu A_2}$ or $\Delta\hat{\tau} = \hat{\tau}_{B_1 h_\mu} - \hat{\tau}_{B_2 h_\mu}$). All dots in (f) and (g) can be found along the diagonal lines, confirming acceptable reconstruction. Full integrating analyses for inferring structures (d) and (e) are given in Tables a3 and a4. Here, the complex network is reconstructed based on the network motifs in Figure 1(b) (all blue nodes and links) and Figure 1(c) and (d) (all purple nodes and links).

4 Uncovering hidden nodes and hidden links for network with internal and distributed noises

In the above discussion, injected noises are used to infer dark network structures associated with hidden nodes. This strategy is anticipated to be applicable in several realistic systems. However, there are also some practical cases where signal injections are difficult while internal noises are present and distributed in network nodes. In this work, internally distributed noises have become crucial. This issue can be examined with exactly the same algorithms in sect. 3, where, however, internal noises are present not only in accessible nodes but also in hidden nodes, producing additional rich information for network reconstruction.

For internal fast-varying noises, eq. (1a) is replaced by

$$\frac{\mathrm{d}x_i(t)}{\mathrm{d}t} = -\frac{1}{\varepsilon}x_i(t)(x_i(t)-1)\left(x_i(t)-\frac{y_i(t)+b}{a}\right) + \sum_{j=1,j\neq i}^{N} w_{ij}\left(x_j\left(t-\hat{\tau}_{ij}\right)-x_i(t)\right)+\Gamma_i(t), \tag{7}$$

with nodes $i = 1, 2, \cdots, M < N$ being measurable and nodes $i = M+1, \cdots, N$ being hidden. Because distributed noises derived from the microscopic world have a much shorter correlation time compared with the characteristic time of macroscopic network dynamics, white noise approximations are adopted

$$\left\langle \Gamma_i(t)\Gamma_j(t+t')\right\rangle = Q_i\delta_{ij}\delta(t'). \tag{8}$$

Note the intensities of Q_i are unknown, but all Q_i for accessible nodes can be easily determined, based on available data $Q_i = \frac{1}{L}\sum_{k=1}^{L} x_i^{(1)}(t_k)x_i^{(1)}(t_k)\Delta t$. With data of two measurable nodes A and B (eq. (2c)), we can follow all the computation procedures of eqs. (3)-(5). Then, all the internally distributed noises serve as the signal sources in eq. (5) for reconstruction of hidden nodes and dark interaction structure. The only difference is that one may observe more peaks in $E_{BA}^{d+1,1}(t')$,

inferring more information from all noise signal sources including noises in both accessible nodes and in hidden nodes along all paths between these two accessible nodes. For a direct interaction ($d = 1$) between two accessible nodes, eq. (5) is changed to

$$E_{BA}^{2,1}(t') = \begin{cases} 0(\Delta t), & t'_k \neq \tau_{BA}, -\tau_{AB}, \\ Q_A I_{BA} + 0(\Delta t), & t'_k = \tau_{BA}, \\ -Q_B I_{AB} + 0(\Delta t), & t'_k = -\tau_{AB}. \end{cases} \tag{9}$$

Two peaks caused by internal noises in both nodes A and B may exist at right positions, if there are bi-direct interactions between A and B. For $d = 2$ indirect interaction path with a hidden node h in between A and B, we have

$$E_{BA}^{3,1}(t') = \begin{cases} 0(\Delta t), & t'_k \neq \tau_{BA}(2), -\tau_{AB}(2), \tau_{Ah} - \tau_{Bh}, \\ Q_A I_{BA}(2) + 0(\Delta t), & t'_k = \tau_{BA}(2), \\ Q_B I_{AB}(2) + 0(\Delta t), & t'_k = -\tau_{AB}(2), \\ -Q_h I_{Ah} I_{Bh} + 0(\Delta t), & t'_k = \tau_{Ah} - \tau_{Bh}. \end{cases} \tag{10}$$

A general correlation form for path of distance d $A \to h_1 \to \cdots \to h_\nu \to h_{(d-1)} \to B$ reads

$$E_{BA}^{d+1,1}(t') = \begin{cases} 0(\Delta t), & t'_k \neq \text{all the following specific values}, \\ Q_A I_{BA}(d) + 0(\Delta t), & t'_k = \tau_{BA}(d), \\ (-1)^d Q_B I_{AB}(d) + 0(\Delta t), & t'_k = -\tau_{AB}(d), \\ \vdots & \\ (-1)^\nu Q_{h_\nu} I_{Ah_\nu}(\nu) I_{Bh_\nu}(d-\nu) + 0(\Delta t), & t'_k = \tau_{Ah_\nu}(\nu) - \tau_{Bh_\nu}(d-\nu), \\ \vdots & \\ (-1)^{d-1} Q_{h_{d-1}} I_{Ah_{d-1}}(d-1) I_{Bh_{d-1}}(1) + 0(\Delta t) & t'_k = \tau_{Ah_{d-1}}(d-1) - \tau_{Bh_1}(1). \end{cases} \tag{11}$$

Unlike eq. (5), where only a single peak is generated by the injected noise for any path of various distance d's, in eq. (11) for a path of length d, $d+1$ peaks result in noises distributed in the $d+1$ nodes. All our task is to reconstruct the quantities of $\hat{I}_{BA}(d_{BA})$ and $\hat{\tau}_{BA}(d_{BA})$ by eqs. (3)-(11) and integrate these reconstructed quantities for different pairs of accessible nodes to brighten up hidden nodes and their hidden structure in the whole network. In Figure 3(a), another reconstruction motif is shown for $d = d' = 2$ (interactions with orange color aside from the same-colored node) under the condition of distributed noises, additional to the motif structure of Figure 1(b). By using eq. (6c) and the last line of eq. (10) and considering peak quantities in Figure 3(b),

$$\tau_{B_1A}(2) - \tau_{B_2A}(2) = \tau_{B_2B_1}(2) = \tau_{B_1h}(1) - \tau_{B_2h}(1), \tag{12}$$

which definitely recognizes the hidden node h with its input $A \to h$ and outputs $h \to B_1, B_2$ based on the novel signal peak offered by noise in the hidden node h (the peak in the bottom panel of Figure 3(b)).

In Figure 3(c), we do exactly the same as in Figure 2, with internal and distributed noises applying in eq. (7) (for comparison, we use $Q_i = Q_A = 0.2$). By using $d = 2$ correlations and the motif in Figure 1(b), blue hidden nodes and links can also be inferred in Figure 3(c). By taking into consideration the motif in Figure 3(a), additional orange hidden nodes and hidden links in Figure 3(c) are determined without further consideration of $d = 3$ correlations. By comparison with Tables a1 and a3, peak heights and peak positions of $E_{BA}^{d+1,1}(t')/Q_A$ correlation curves in eq. (5) with $d = 2$ in Table a5 for the network of Figure 2(a) with internally distributed noises eq. (7) are presented. The reconstructed results align well with the actual ones. It is evident that all data in Table a1 appear in Table a5 approximately, demonstrating that the analyses applied by the noise injection approach also work for internal and distributed noises. Moreover, this observation indicates wide applications of our reconstruction approach in realistic systems. A fascinating observation is that noises in hidden nodes could offer more information for network inference (underline quantities in Table a5). In Table a6, we go further to do the same as in Table a3 for uncovering hidden nodes and hidden links by using $d = d' = 2$ motifs only, where some hidden nodes (nodes 17, 18, 19) and the associated interactions in orange color, which cannot be examined with injected noises in Table a3, can be clearly reconstructed in Table a6, with only $d = 2$ correlation calculation of accessible node pairs using the motif in Figure 3(a) (i.e., by signals from noises in the hidden nodes).

5 Conclusion

In conclusion, a method for analyzing singularities caused

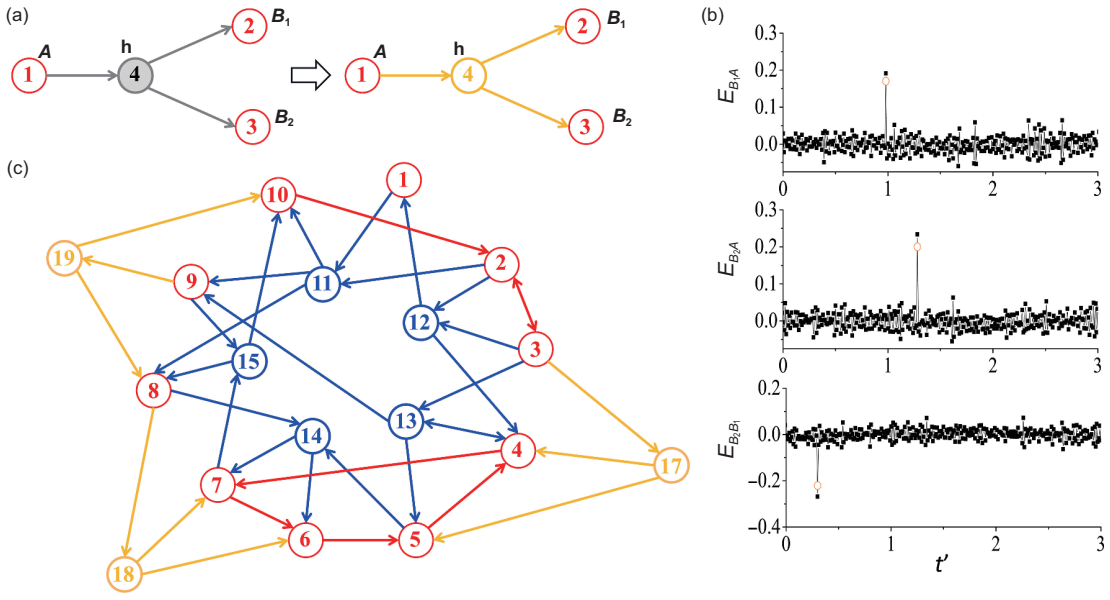

Figure 3 Reconstructing a complex network with internally distributed noises. (a) Another reconstruction motif of $d = d' = 2$, additional to the motif in Figure 1(b), based also on $d = d' = 2$ correlation computation in eqs. (6c) and (10). Hidden node 4 and its input and outputs could be fixed by correlations definitely. (b) Some $E_{BA}^{d+1,1}(t')$ curves plotted against t' for $d = 2$. Data are produced by the motif network in (a) with internal noises distributed in all network nodes, $Q_i = 0.2, i = 1, 2, \cdots, 4$. By applying eq. (10) for $E_{B_1A}^{d+1,1}(t')$, $E_{B_2A}^{d+1,1}(t')$, $E_{B_2B_1}^{d+1,1}(t')$ with $d = 2$ for multiple pairs of accessible nodes, a new reconstruction motif can be defined in (a). (c) Reconstructing the network structure of Figure 2(a) under internally distributed noises with correlations upper to $d = 2$. All blue hidden nodes and links are acquired by the noise signals from accessible nodes, while orange hidden nodes and links are reconstructed with the signals (peaks of correlation $E_{A_1A_2}^{3,1}(t')$) from noises in the hidden nodes. All the associated quantities are given in Tables a5 and a6, where noises in the hidden nodes contribute more peak signals in Table a5, and motif (a) infers additional hidden nodes and hidden links in Table a6.

by fast-varying noises, both externally injected to or internally present in network nodes, is developed to uncover hidden nodes and the associated hidden structure in the network. By calculation of the correlations of measurable data for multiple pairs of accessible nodes with different derivative orders (eqs. (3)-(5), (7)-(12)) and finding out quantitative relations between various correlations with use of reconstruction motifs in Figures 1(b)-(d) and 3(a), the hidden world of networks is successfully brightened by recognizing hidden nodes, examining the interaction structure between hidden nodes and accessible nodes, and calculating the quantities of all links inputting to and outputting from any hidden node explored. All the analysis here dealts with linear diffusive couplings. The approach can also be applied to nonlinear chemical synapses for neural networks. Moreover, the identities for interaction intensities no longer work; however, those for time delays work equally in hidden network reconstruction.

It is emphasized that though in this paper, correlations $E_{BA}^{d+1,1}(t')$ were analyzed for $d = 1, 2$ and 3 only (Figure 2, 3, and Tables a1-a6), all correlations of different d involve possibly independent information, and synthesizing the findings of even large $d's$ can aid in inferring hidden nodes and hidden structure in more difficult conditions, that is, to examine larger numbers of hidden nodes with smaller part of accessible nodes in networks.

In all eqs. (3)–(12), white noises play an active role in the reconstruction of hidden nodes and their associated interaction structure. However, noises also play negative roles in causing random fluctuations, destroying the active signals. In theory, this issue can surely be addressed when sufficiently high-frequency measurements ($\triangle t \ll 1$) are employed, and large data sets ($L \gg 1$) are gathered. However, it remains a great challenge to increase the reconstruction quality of hidden nodes and hidden structures, given limited measurement frequencies and available data in real measurements.

In several realistic networks, some units of importance are often not reachable [51-53]. Systematic analyses of these hidden parts according to measurable, accessible data can help understand and control the whole network structures and the network functions [9, 54]. Applications of the theoretical approaches to some practically important systems according to real data may be future work for network reconstruction research.

Gang Hu was supported by the National Natural Science Foundation of China (Grant No. 11835003). Zhaoyang Zhang was supported by the National Natural Science Foundation of China (Grant Nos. 12375033, 12235007, and 11975131), the Natural Science Foundation of Zhejiang (Grant No. LY23A050002), and the K. C. Wong Magna Fund at Ningbo University. Yuanyuan Mi was supported by the National Natural Science Foundation of China (Grant No. T2122016), the National Science and Technology Innovation 2030 Major Program (Grant Nos. 2021ZD0203700, and

2021ZD0203705), the Fundamental Research Funds for the Central Universities (Grant No. 2022CDJKYJH034). Zhilin Qu was supported by the National Institutes of Health (Grant Nos. R01 HL134709, R01 HL139829, R01 HL157116, and P01 HL164311). Yang Chen was supported by the National Natural Science Foundation of China (Grant No. 11905291), and CAS Project for Young Scientists in Basic Research (Grant No. YSBR-041).

1 T. S. Gardner, D. di Bernardo, D. Lorenz, and J. J. Collins, Science **301**, 102 (2003).
2 M. Timme, Phys. Rev. Lett. **98**, 224101 (2007).
3 J. Ren, W. X. Wang, B. Li, and Y. C. Lai, Phys. Rev. Lett. **104**, 058701 (2010).
4 W. X. Wang, R. Yang, Y. C. Lai, V. Kovanis, and C. Grebogi, Phys. Rev. Lett. **106**, 154101 (2011).
5 S. Hempel, A. Koseska, J. Kurths, and Z. Nikoloski, Phys. Rev. Lett. **107**, 054101 (2011).
6 Z. Levnajić, and A. Pikovsky, Phys. Rev. Lett. **107**, 034101 (2011).
7 D. Marbach, J. C. Costello, R. Küffner, N. M. Vega, R. J. Prill, D. M. Camacho, K. R. Allison, M. Kellis, J. J. Collins, and G. Stolovitzky, Nat. Methods **9**, 796 (2012).
8 X. Han, Z. Shen, W. X. Wang, and Z. Di, Phys. Rev. Lett. **114**, 028701 (2015).
9 W. X. Wang, Y. C. Lai, and C. Grebogi, Phys. Rep. **644**, 1 (2016).
10 J. Casadiego, M. Nitzan, S. Hallerberg, and M. Timme, Nat. Commun. **8**, 2192 (2017).
11 J. Casadiego, D. Maoutsa, and M. Timme, Phys. Rev. Lett. **121**, 054101 (2018).
12 A. Banerjee, J. D. Hart, R. Roy, and E. Ott, Phys. Rev. X **11**, 031014 (2021).
13 K. Srinivasan, N. Coble, J. Hamlin, T. Antonsen, E. Ott, and M. Girvan, Phys. Rev. Lett. **128**, 164101 (2022).
14 T. T. Gao, and G. Yan, Nat. Comput. Sci. **2**, 160 (2022).
15 A. K. Fletcher, and S. Rangan, in *Scalable inference for neuronal connectivity from calcium imaging: Advances in Neural Information Processing Systems*, edited by Z. Ghahramani, M. Welling, C. Cortes, N. Lawrence, and K. Weinberger, Vol. 27 (Curran Associates, Inc., 2014).
16 L. Aitchison, L. Russell, A. M. Packer, J. Yan, P. Castonguay, M. Hausser, and S. C. Turaga, in *Model-based Bayesian inference of neural activity and connectivity from all-optical interrogation of a neural circuit: Advances in Neural Information Processing Systems*, edited by I. Guyon, U. V. Luxburg, S. Bengio, H. Wallach, R. Fergus, S. Vishwanathan, and R. Garnett, Vol. 30 (Curran Associates, Inc., 2017).
17 I. Magrans de Abril, J. Yoshimoto, and K. Doya, Neural Networks **102**, 120 (2018).
18 A. Banerjee, S. Chandra, and E. Ott, Proc. Natl. Acad. Sci. USA **120**, e2216030120 (2023).
19 R. Q. Su, W. X. Wang, and Y. C. Lai, Phys. Rev. E **85**, 065201 (2012).
20 R. Q. Su, Y. C. Lai, X. Wang, and Y. Do, Sci. Rep. **4**, 3944 (2014).
21 Z. Shen, W. X. Wang, Y. Fan, Z. Di, and Y. C. Lai, Nat. Commun. **5**, 4323 (2014).
22 M. Porfiri, Phys. Rev. Lett. **124**, 168301 (2020).
23 H. Haehne, J. Casadiego, J. Peinke, and M. Timme, Phys. Rev. Lett. **122**, 158301 (2019).
24 E. S. C. Ching, and P. H. Tam, Phys. Rev. E **98**, 062318 (2018).
25 B. Gemao, and P. Y. Lai, Phys. Rev. E **103**, 062302 (2021).
26 R. Schmidt, H. Haehne, L. Hillmann, J. Casadiego, D. Witthaut, B. Schafer, and M. Timme, IEEE Access **10**, 76682 (2022).
27 S. Lee, V. Periwal, and J. Jo, Phys. Rev. E **104**, 024119 (2021).
28 D. T. Hoang, J. Jo, and V. Periwal, Phys. Rev. E **99**, 042114 (2019).
29 B. Dunn, and Y. Roudi, Phys. Rev. E **87**, 022127 (2013).
30 X. Wang, Y. Mi, Z. Zhang, Y. Chen, G. Hu, and H. Li, Phys. Rev. E **106**, 014302 (2022).
31 M. Tyloo, R. Delabays, and P. Jacquod, Chaos-An Interdiscip. J. Nonlinear Sci. **31**, 103117 (2021).
32 B. Lindner, Phys. Rep. **392**, 321 (2004).
33 J. A. White, J. T. Rubinstein, and A. R. Kay, Trends Neurosci. **23**, 131 (2000).
34 A. A. Faisal, L. P. J. Selen, and D. M. Wolpert, Nat. Rev. Neurosci. **9**, 292 (2008).
35 C. A. A. de Carvalho, and H. M. Nussenzveig, Phys. Rep. **364**, 83 (2002).
36 K. K. Sreenivasan, and M. D'Esposito, Nat. Rev. Neurosci. **20**, 466 (2019).
37 S. Leng, H. Ma, J. Kurths, Y. C. Lai, W. Lin, K. Aihara, and L. Chen, Nat. Commun. **11**, 2632 (2020).
38 H. Ma, S. Leng, C. Tao, X. Ying, J. Kurths, Y. C. Lai, and W. Lin, Phys. Rev. E **96**, 012221 (2017).
39 C. Hens, U. Harush, S. Haber, R. Cohen, and B. Barzel, Nat. Phys. **15**, 403 (2019).
40 Z. Zhang, G. Hu, Y. Zhang, and Z. Qu, Phys. Rev. Lett. **129**, 048101 (2022).
41 D. Q. Nykamp, Phys. Rev. E **78**, 021902 (2008).
42 D. Soudry, S. Keshri, P. Stinson, M.-h. Oh, G. Iyengar, and L. Paninski, PLOS Comput. Bio. **11**, e1004657 (2015).
43 B. A. W. Brinkman, F. Rieke, E. Shea-Brown, and M. A. Buice, PLOS Comput. Bio. **14**, e1006490 (2018).
44 A. Das, and I. R. Fiete, Nat. Neurosci. **23**, 1286 (2020).
45 W. Gilpin, Y. Huang, and D. B. Forger, Curr. Opin. Syst. Biol. **22**, 1 (2020).
46 S. Panzeri, M. Moroni, H. Safaai, and C. D. Harvey, Nat. Rev. Neurosci. **23**, 551 (2022).
47 X. Liao, Q. Xia, Y. Qian, L. Zhang, G. Hu, and Y. Mi, Phys. Rev. E **83**, 056204 (2011).
48 Y. Qian, X. Huang, G. Hu, and X. Liao, Phys. Rev. E **81**, 036101 (2010).
49 Z. Zhang, Z. Zheng, H. Niu, Y. Mi, S. Wu, and G. Hu, Phys. Rev. E **91**, 012814 (2015).
50 Z. Zhang, Y. Chen, Y. Mi, and G. Hu, Phys. Rev. E **99**, 042311 (2019).
51 A. Levina, V. Priesemann, and J. Zierenberg, Nat. Rev. Phys. **4**, 770 (2022).
52 J. van der Meer, B. Ertel, and U. Seifert, Phys. Rev. X **12**, 031025 (2022).
53 P. E. Harunari, A. Dutta, M. Polettini, and É. Roldán, Phys. Rev. X **12**, 041026 (2022).
54 C. Liu, Y. Ma, J. Zhao, R. Nussinov, Y. C. Zhang, F. Cheng, and Z. K. Zhang, Phys. Rep. **846**, 1 (2020).

Appendix

Table a1 Peak heights/positions of $E_{BA}^{d+1,1}(t')/Q_A$ curves (quantities of Roman type, $I_{BA}(2)/(\tau_{BA}(2)/\Delta t)$) for $d = 2$ for all accessible A nodes (vertical nodes 1-10 in Figure 2(b)) and B ($B \neq A$) nodes (horizontal nodes 1-10 in Figure 2(b)). All *italic* quantities show actual $\hat{I}_{BA}(2)/(\hat{\tau}_{BA}(2)/\Delta t)$ in the network eq. (1). All black quantities infer $d = 2$ paths passing through a hidden node. In some grids for $d = 2$, multiple data pairs represent multiple paths between the given pair of (A, B) nodes through different hidden nodes. For example, as there is only one path with $d = 2$ from node 3 to hidden node 13 then to node 9, in grid (3, 9) the quantity of Roman type shows peak height of $E_{9,3}^{3,1}(\tau')/Q_A = I_{9,3}(2) = 0.993$ and peak position $\tau_{9,3}(2)/\Delta t = 96$ while the quantities of *italic* type $\hat{I}_{9,3}(2)$=1.011 and $\hat{\tau}(2)/\Delta t = 96$ are in eqs. (1), (4a), (4b). All reconstructed quantities of Roman type satisfactorily reproduce actual ones of *italic* type

A	Interaction intensities/total time delays $\tau_{BA}/\Delta t$ for $d = 2$ interaction paths									
	B=1	B=2	B=3	B=4	B=5	B=6	B=7	B=8	B=9	B=10
1	–	–	1.046/142	–	–	–	–	0.891/120	0.971/70	1.225/174
	–	–	*1.109/142*	–	–	–	–	*– 0.906/120*	*0.969/70*	*1.280/174*
	–	–	–	–	–	–	–	–	–	0.972/122
	–	–	–	–	–	–	–	–	–	*0.994/122*
2	0.709/124	–	0.963/182	0.678/126	–	–	–	0.874/130	0.932/80	0.941/132
	0.727/124	–	*0.929/182*	*0.691/126*	–	–	–	*0.888/130*	*0.950/80*	*0.975/132*
3	0.825/138	–	–	0.843/166	1.180/146	–	–	–	0.993/96	–
	0.825/138	–	–	*0.894/166*	*1.210/146*	–	–	–	*1.011/96*	–
	–	–	–	0.749/140	1.137/114	–	–	–	–	–
	–	–	–	*0.785/140*	*1.134/114*	–	–	–	–	–
	–	–	–	1.192/82	–	–	–	–	–	–
	–	–	–	*1.208/82*	–	–	–	–	–	–
4	–	–	–	–	1.323/138	–	–	–	1.091/88	–
	–	–	–	–	*1.303/138*	–	–	–	*1.088/88*	–
5	–	–	–	–	–	1.335/132	1.009/110	–	–	–
	–	–	–	–	–	*1.321/132*	1.019/110	–	–	–
6	–	–	–	–	–	–	–	–	–	–
	–	–	–	–	–	–	–	–	–	–
7	–	–	–	–	–	–	–	0.946/84	–	1.061/66
	–	–	–	–	–	–	–	*0.979/84*	–	*1.093/66*
8	–	–	–	–	–	0.850/188	0.659/152	–	–	–
	–	–	–	–	–	*0.949/188*	*0.754/152*	–	–	–
	–	–	–	–	–	0.930/144	0.710/122	–	–	–
	–	–	–	–	–	*0.945/144*	*0.729/122*	–	–	–
9	–	–	–	–	–	–	–	0.901/142	–	1.034/184
	–	–	–	–	–	–	–	*0.978/142*	–	*1.086/184*
	–	–	–	–	–	–	–	0.945/126	–	0.791/180
	–	–	–	–	–	–	–	*1.005/126*	–	*0.802/180*
	–	–	–	–	–	–	–	–	–	1.071/124
	–	–	–	–	–	–	–	–	–	*1.092/124*
10	–	–	–	–	–	–	–	1.264/116	–	–
	–	–	–	–	–	–	–	*1.246/116*	–	–

Table a2 The same as Table a1 with $d = 3$ interaction paths considered and computed with two hidden nodes in the paths

A	Interaction intensities/total time delays $\tau_{BA}/\Delta t$ for $d = 3$ interaction paths									
	B=1	B=2	B=3	B=4	B=5	B=6	B=7	B=8	B=9	B=10
1	–	–	–	1.099/214	1.422/194	–	–	1.263/224	1.244/144	1.000/278
	–	–	–	*1.053/214*	*1.424/194*	–	–	*1.319/224*	*1.190/144*	*1.053/278*
	–	–	–	1.132/114	0.969/146	–	–	1.027/164	–	1.149/146
	–	–	–	*1.161/114*	*1.090/146*	–	–	*1.058/164*	–	*1.181/146*
2	–	–	–	1.013/224	1.291/204	–	–	1.055/174	1.325/154	0.845/156
	–	–	–	*1.033/224*	*1.397/204*	–	–	*1.038/174*	*1.167/154*	*1.158/156*
	–	–	–	0.798/154	0.850/186	–	–	–	–	–
	–	–	–	*0.972/154*	*0.913/186*	–	–	–	–	–
3	–	–	–	–	–	–	–	0.921/188	1.080/138	1.068/190
	–	–	–	–	–	–	–	*0.987/188*	*1.056/138*	*1.083/190*
4	–	–	–	–	–	–	–	0.906/180	1.091/130	1.088/182
	–	–	–	–	–	–	–	*1.063/180*	*1.137/130*	*1.167/182*
5	0.901/174	–	–	–	–	–	–	–	–	–
	1.029/174	–	–	*0.978/176*	–	–	–	–	–	–
6	–	–	–	–	–	–	–	–	–	–
7	–	–	–	–	–	–	–	–	–	–
8	0.963/186	–	–	0.609/188	–	–	–	–	–	–
	0.736/186	–	–	*0.700/188*	–	–	–	–	–	–
9	–	–	–	–	–	1.005/240	0.788/204	1.183/234	–	1.147/288
	–	–	–	–	–	*1.141/240*	*0.907/204*	*1.120/234*	–	*0.894/288*
10	–	–	–	–	–	1.490/230	1.132/194	–	–	–
	–	–	–	–	–	*1.415/230*	*1.125/194*	–	–	–

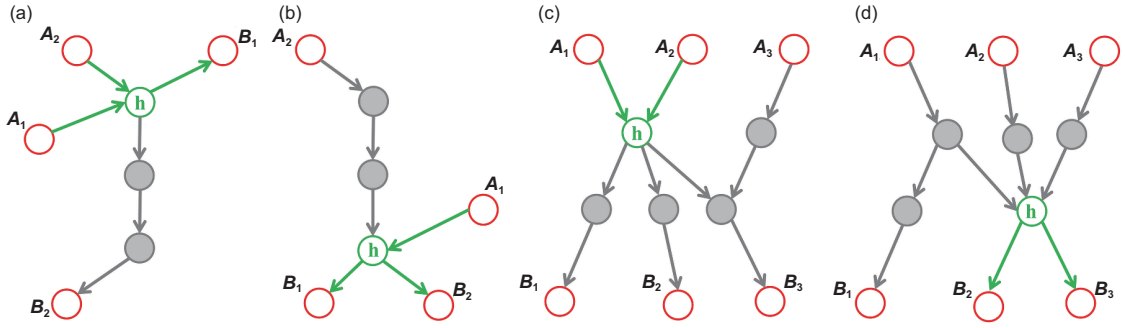

Figure a1 Four motifs for distances of interactions larger than those of motifs in Figure 1(b)-(d). All green nodes and links are identified by the given motifs. Motifs with even large $d's$ can be also found in the similar manner.

Table a3 The same as Table a1 for reconstructed results with black data in Table a1 replaced by blue and purple colors, indicating that we have uniquely explored the numbered hidden nodes (the particular numbers of hidden nodes in brackets are adopted from Figure 2(a)) with all its inputs and outputs. Blue colored results are obtained by analyzing Table a1 only for $d = d' = 2$ in eq. (6) with network motif in Figure 1(b) (shown in Figure 2(d)), and purple colored ones by integrating data in both Tables a1, a2 and applying eq. (6) for $d = 2$, $d' = 3$ with network motifs in Figure 1(c) and (d) (shown in Figure 2(e))

A	Uncovering hidden node and hidden links in Table a1									
	B=1	B=2	B=3	B=4	B=5	B=6	B=7	B=8	B=9	B=10
1	–	–	1.046/142	–	–	–	–	0.891/120	0.971/70	1.225/174
	–	–	(16)	–	–	–	–	(11)	(11)	(20)
	–	–	–	–	–	–	–	–	–	0.972/122
	–	–	–	–	–	–	–	–	–	(11)
2	0.709/124	–	0.963/182	0.678/126	–	–	–	0.874/130	0.932/80	0.941/132
	(12)	–	(16)	(12)	–	–	–	(11)	(11)	(11)
3	0.825/138	–	–	0.843/166	1.180/146	–	–	–	0.993/96	–
	(12)	–	–	(13)	(13)	–	–	–	(13)	–
	–	–	–	0.749/140	1.137/114	–	–	–	–	–
	–	–	–	(12)	(17)	–	–	–	–	–
	–	–	–	1.192/82	–	–	–	–	–	–
	–	–	–	(17)	–	–	–	–	–	–
4	–	–	–	–	1.323/138	–	–	–	1.091/88	–
	–	–	–	–	(13)	–	–	–	(13)	–
5	–	–	–	–	–	1.335/132	1.009/110	–	–	–
	–	–	–	–	–	(14)	(14)	–	–	–
6	–	–	–	–	–	–	–	–	–	–
7	–	–	–	–	–	–	–	0.946/84	–	1.061/66
	–	–	–	–	–	–	–	(15)	–	(15)
8	–	–	–	–	–	0.850/188	0.659/152	–	–	–
	–	–	–	–	–	(18)	(18)	–	–	–
	–	–	–	–	–	0.930/144	0.710/122	–	–	–
	–	–	–	–	–	(14)	(14)	–	–	–
9	–	–	–	–	–	–	–	0.901/142	–	1.034/184
	–	–	–	–	–	–	–	(15)	–	(20)
	–	–	–	–	–	–	–	0.945/126	–	0.791/180
	–	–	–	–	–	–	–	(19)	–	(19)
	–	–	–	–	–	–	–	–	–	1.071/124
	–	–	–	–	–	–	–	–	–	(15)
10	–	–	–	–	–	–	–	1.264/116	–	–
	–	–	–	–	–	–	–	(19)	–	–

Table a4 The same as Table a3 with $d = 3$ interaction paths considered. Here, purple numbers integrate and synthesize data in both Tables a1 and a2 by applying network motifs in Figure 1(c) and (d), and the purple numbers in Tables a3 and a4 definitely construct all purple part of hidden nodes and hidden network structure of Figure 2(e). Moreover, the blue numbers in Table a3 and purple numbers in both Tables a3 and this table together perform complete recovery of the hidden part of network Figure 2(a)

A	Uncovering hidden node and hidden links in Table a2									
	B=1	B=2	B=3	B=4	B=5	B=6	B=7	B=8	B=9	B=10
1	–	–	–	1.099/214	1.422/194	–	–	1.263/224	1.244/144	1.000/278
	–	–	–	(11,13)	(11,13)	–	–	(20,19)	(11,13)	(20,19)
	–	–	–	1.132/114	0.969/146	–	–	1.027/164	–	1.149/146
	–	–	–	(16,17)	(16,17)	–	–	(11,15)	–	(11,15)
2	–	–	–	1.013/224	1.291/204	–	–	1.055/174	1.325/154	0.845/156
	–	–	–	(11,13)	(11,13)	–	–	(11,15)	(11,13)	(11,15)
	–	–	–	0.798/154	0.850/186	–	–	–	–	–
	–	–	–	(16,17)	(16,17)	–	–	–	–	–
3	–	–	–	–	–	–	–	0.921/188	1.080/138	1.068/190
	–	–	–	–	–	–	–	(13,11)	(13,11)	(13,11)
4	–	–	–	–	–	–	–	0.906/180	1.091/130	1.088/182
	–	–	–	–	–	–	–	(13,11)	(13,11)	(13,11)
5	0.901/174	–	–	–	–	–	–	–	–	–
	(14,12)	–	–	–	–	–	–	–	–	–
6	–	–	–	–	–	–	–	–	–	–
7	–	–	–	–	–	–	–	–	–	–
8	0.963/186	–	–	0.609/188	–	–	–	–	–	–
	(14,12)	–	–	(14,12)	–	–	–	–	–	–
9	–	–	–	–	–	1.005/240	0.788/204	1.183/234	–	1.147/288
	–	–	–	–	–	(19,18)	(19,18)	(20,19)	–	(20,19)
10	–	–	–	–	–	1.490/230	1.132/194	–	–	–
	–	–	–	–	–	(19,18)	(19,18)	–	–	–

Table a5 The same as Table a1 with internal and distributed noises eq. (7) considered. For a comparison with Table a1, we take $Q_i = 0.2, i = 1, 2, ..., 20$. All quantities in Table a1 appear approximately in this table (quantities without underline). The additional quantities with underline in this table are taken from peaks produced by noises in hidden nodes. Note, in this table only peaks with positive time-delay are shown. There are other peaks, symmetric to those peaks and not adding any novel information, are not shown. This rule is also followed in Table a6

A	Interaction intensities/total time delays $\tau_{BA}/\Delta t$ for $d = 2$ interaction paths in distributed noises									
	B=1	B=2	B=3	B=4	B=5	B=6	B=7	B=8	B=9	B=10
1	–	–	1.191/142	–0.764/2	–	–	–	0.842/120	0.982/70	1.282/174
	–	–	–	–	–	–	–	–	–	1.096/122
2	0.679/124	–	0.884/182	0.607/126	–	–	–	0.935/130	0.788/80	1.020/132
3	0.745/138	–	–	0.971/166	1.113/146	–	–	–	1.012/96	–
	–	–	–	0.854/140	1.110/114	–	–	–	–	–
	–	–	–	1.084/82	–	–	–	–	–	–
4	–	–	–	–	1.171/138	–	–	–	0.998/88	–
	–	–	–	–	–1.350/32	–	–	–	–	–
5	–	–	–	–0.998/20	–	1.364/132	1.066/110	–	–	–
6	–	–	–	–	–	–	–	–	–	–
7	–	–	–	–	–	–0.966/22	–	0.941/84	–	1.014/66
	–	–	–	–	–	–1.279/36	–	–	–	–
8	–	–	–	–	–	0.928/188	0.626/152	–	–	–0.783/2
	–	–	–	–	–	0.861/144	0.748/122	–	–	–1.118/54
9	–	–	–	–0.916/70	–1.054/50	–	–	0.901/142	–	1.008/184
	–	–	–	–	–	–	–	1.011/126	–	0.792/180
	–	–	–	–	–	–	–	–0.908/50	–	1.113/124
	–	–	–	–	–	–	–	–	–	–0.893/52
10	–	–	–	–	–	–	–	1.118/116	–	–
	–	–	–	–	–	–	–	–0.876/18	–	–

Table a6 The same as Table a3 with internal and distributed noises considered. All blue quantities are identical to the ones in Table a3, which are reconstructed by eq. (6) and motif in Figure 1(b). All orange data, with or without underline, provide additional information of hidden structures. Interestingly, hidden nodes 17, 18, 19 and the related interactions, which cannot be identified in Table a3, are definitely inferred with the information generated by noise sources of hidden nodes and by applying the motif in Figure 3(a). All the remaining black quantities and hidden nodes 16, 20 could not be inferred with correlations upper to $d = 2$

A	Uncovering hidden node and hidden links in Table a5									
	B=1	B=2	B=3	B=4	B=5	B=6	B=7	B=8	B=9	B=10
1	–	–	1.191/142	–0.764/2	–	–	–	0.842/120	0.982/70	1.282/174
	–	–		(12)	–	–	–	(11)	(11)	
	–	–	–	–	–	–	–	–	–	1.096/122
	–	–	–	–	–	–	–	–	–	(11)
2	0.679/124	–	0.884/182	0.607/126	–	–	–	0.935/130	0.788/80	1.020/132
	(12)	–		(12)	–	–	–	(11)	(11)	(11)
3	0.745/138	–	–	0.971/166	1.113/146	–	–	–	1.012/96	–
	(12)	–	–	(13)	(13)	–	–	–	(13)	–
	–	–	–	0.854/140	1.110/114	–	–	–	–	–
	–	–	–	(12)	(17)	–	–	–	–	–
	–	–	–	1.084/82	–	–	–	–	–	–
	–	–	–	(17)	–	–	–	–	–	–
4	–	–	–	–	1.171/138	–	–	–	0.998/88	–
	–	–	–	–	(13)	–	–	–	(13)	–
	–	–	–	–	–1.350/32	–	–	–	–	–
	–	–	–	–	(17)	–	–	–	–	–
5	–	–	–	–0.998/20	–	1.364/132	1.066/110	–	–	–
	–	–	–	(13)	–	(14)	(14)	–	–	–
6	–	–	–	–	–	–	–	–	–	–
7	–	–	–	–	–	–0.966/22	–	0.941/84	–	1.014/66
	–	–	–	–	–	(14)	–	(15)	–	(15)
	–	–	–	–	–	–1.279/36	–	–	–	–
	–	–	–	–	–	(18)	–	–	–	–
8	–	–	–	–	–	0.928/188	0.626/152	–	–	–0.783/2
	–	–	–	–	–	(18)	(18)	–	–	(11)
	–	–	–	–	–	0.861/144	0.748/122	–	–	–1.118/54
	–	–	–	–	–	(14)	(14)	–	–	(19)
9	–	–	–	–0.916/70	–1.054/50	–	–	0.901/142	–	1.008/184
	–	–	–	(13)	(13)	–	–	(15)	–	
	–	–	–	–	–	–	–	1.011/126	–	0.792/180
	–	–	–	–	–	–	–	(19)	–	(19)
	–	–	–	–	–	–	–	–0.908/50	–	1.113/124
	–	–	–	–	–	–	–	(11)	–	(15)
	–	–	–	–	–	–	–	–	–	–0.893/52
	–	–	–	–	–	–	–	–	–	(11)
10	–	–	–	–	–	–	–	1.118/116	–	–
	–	–	–	–	–	–	–		–	–
	–	–	–	–	–	–	–	–0.876/18	–	–
	–	–	–	–	–	–	–	(15)	–	–